NASA
Technical Paper 1810

AVRADCOM
Technical Report 80-C-17



# Reasons for Low Aerodynamic Performance of 13.5-Centimeter-Tip-Diameter Aircraft Engine Starter Turbine

Jeffrey E. Haas, Richard J. Roelke,
and Paul Hermann

MARCH 1981

NASA

U.S. ARMY AVRADCOM

NASA
Technical Paper 1810

AVRADCOM
Technical Report 80-C-17

# Reasons for Low Aerodynamic Performance of 13.5-Centimeter-Tip-Diameter Aircraft Engine Starter Turbine

Jeffrey E. Haas
*Propulsion Laboratory*
*AVRADCOM Research and Technology Laboratories*
*Lewis Research Center*
*Cleveland, Ohio*

Richard J. Roelke
*Lewis Research Center*
*Cleveland, Ohio*

Paul Hermann
*Sundstrand Corporation*
*Rockford, Illinois*

National Aeronautics
and Space Administration

**Scientific and Technical
Information Branch**

1981

## Summary

An experimental investigation was conducted on a 13.5-centimeter-tip-diameter aircraft engine starter turbine to determine the reasons for its low aerodynamic performance. The investigation consisted of an evaluation of both the stator and the stage. The investigation focused on determining the effect on the aerodynamic performance of two turbine design features: the use of a manifold having a single inlet and designed to turn the flow 180° into the stator, and the use of a honeycomb shroud surface over the rotor blade tips. Three rotor configurations and three honeycomb shroud configurations were evaluated. The three rotor configurations consisted of an untwisted, 37-blade rotor, an untwisted, 43-blade rotor, and a twisted, 43-blade rotor. The three honeycomb shroud configurations consisted of the original shroud, a filled shroud, and a half-depth shroud.

The results of this investigation indicated that when the original honeycomb shroud was filled to obtain a solid shroud surface, efficiency improvements ranging from 8.2 to 11.0 points were obtained for the three rotor configurations. As a result the total efficiencies ranged from 0.868 to 0.883. This large loss associated with the open honeycomb shroud was believed to be due primarily to the energy loss associated with gas being transported into and out of the honeycomb cells as a result of the blade-to-blade pressure differential at the tip section.

The effect of the manifold design was to cause large radial and circumferential gradients in flow. However, the stator exit surveys indicated that no major loss areas existed in the stator.


## Introduction

The NASA Lewis Research Center was requested by the Department of the Navy to conduct an experimental performance investigation of a 13.5-centimeter-tip-diameter aircraft engine starter turbine. Experimental evaluation of this turbine by the manufacturer indicated an efficiency that was approximately 10 points lower than design. With this low performance it was believed that this starter turbine could not start the aircraft engine within the time period specified for the aircraft. The experimental program at Lewis was intended to determine the reasons for the turbine performance deficit.

A design review of the turbine at Lewis identified two features that were potential contributors to the observed efficiency deficit. One of these features was the use of a single-inlet manifold designed to turn the flow 180° into the stator. In this kind of manifold design the flow enters a single feed pipe, branches, and then flows down both sides of the manifold, resulting in large and variable stator incidence angles and possibly radial and circumferential gradients in mass flow. The second design feature was the use of a honeycomb shroud surface over the rotor blade tips. The honeycomb was used because it permitted the use of a lower rotor tip clearance and gave protection to the rotor in case of contact with the shroud.

The original starter turbine rotor had 37 untwisted, constant-section blades. Because of the uncertainty as to the cause of the turbine performance deficit, two additional blade designs were made by the manufacturer as possible replacements for the original rotor. Both redesigned rotors had 43 blades to increase blade solidity. One was an untwisted, constant-section blade design and the other was a twisted blade design. All three rotors were delivered to Lewis for experimental evaluation.

The experimental evaluation consisted of two parts: bellmouth inlet and stator exit surveys to determine whether the manifold significantly affected stator performance, and a turbine stage evaluation. Each of the three rotors was evaluated as part of the turbine stage. Each stage configuration was investigated with the original honeycomb shroud configuration and with the honeycomb shroud filled to produce a smooth, continuous shroud surface. In addition, the untwisted, 37-blade rotor configuration was evaluated with a honeycomb shroud configuration that had a cell depth that was half of the original depth.

This report presents the results of the experimental investigation conducted at the Lewis Research Center. Presented are survey results obtained at the bellmouth inlet and stator exit and stage performance results for the different stage configurations investigated. The effect on turbine stage performance of varying the honeycomb depth is also discussed.

## Symbols

| | |
|---|---|
| $AR$ | blade aspect ratio based on actual chord length |
| $N$ | turbine speed, rpm |

$P$ absolute pressure, N/cm$^2$

$R_x$ blade mean reaction, $(P_{2m}-P_{3m})/(P_1-P_{3m})$

$r$ radius, m

$T$ absolute temperature, K

$U$ blade velocity, m/sec

$V$ absolute gas velocity, m/sec

$\Delta V_u$ change in absolute tangential velocity, m/sec

$W$ relative gas velocity, m/sec

$w$ mass flow, kg/sec

$\alpha$ absolute gas flow angle measured from axial direction, deg

$\beta$ relative gas flow angle measured from axial direction, deg

$\gamma$ ratio of specific heats

$\delta$ ratio of manifold inlet total pressure to U.S. standard sea-level pressure, $P_0'/P^*$

$\epsilon$ function of $\gamma$ used in relating parameters to those using air inlet conditions at U.S. standard sea-level conditions, $(0.740/\gamma)[(\gamma+1)/2]^{\gamma/(\gamma-1)}$

$\eta_{0-4}$ static efficiency based on manifold-inlet-total- to diffuser-exit-static-pressure ratio

$\eta_{1-3}$ static efficiency based on bellmouth-inlet-total- to rotor-exit-static pressure ratio

$\eta_{1-3}'$ total efficiency based on bellmouth-inlet- to rotor-exit-total-pressure ratio

$\Delta\eta_{1-3}'$ performance loss

$\theta_{cr}$ squared ratio of critical velocity at manifold inlet temperature to critical velocity at U.S. standard sea-level temperature, $(V_{cr,0}/V_{cr}^*)^2$

$\mu$ viscosity, N sec/m$^2$

$\nu_{0-4}$ blade-jet speed ratio based on manifold-inlet-total- to diffuser-exit-static-pressure ratio

$\nu_{1-3}$ blade-jet speed ratio based on bellmouth-inlet-total- to rotor-exit-static-pressure ratio

$\sigma$ solidity based on actual chord length

Subscripts:

$cr$ condition corresponding to Mach 1

$h$ hub

$m$ mean section

$t$ tip

$u$ tangential direction

0 station at manifold inlet (fig. 7)

1 station at bellmouth inlet (fig. 7)

2 station at stator exit (fig. 7)

3 station at rotor exit (fig. 7)

4 station at diffuser exit (fig. 7)

Superscripts:

$'$ absolute total condition

$*$ U.S. standard sea-level conditions (temperature, 288 K; pressure, 10.13 N/cm$^2$)

## Turbine Design

The aircraft starter turbine tested in this investigation was a single-stage, axial-flow design with a tip diameter of 13.5 centimeters. A cross-section schematic of the turbine is shown in figure 1. Flow entered the manifold at a critical velocity ratio of about 0.25, turned 90°, split, and then turned another 90° into the stator. A short bellmouth inlet was used ahead of the stator to provide minimum inlet endwall boundary layers. The stator vanes were untapered and untwisted. The original rotor blade design was also untwisted but was tapered. A honeycomb material was used over the rotor blades to protect the blades in case of a rotor rub. With this added protection a smaller rotor tip clearance equal to about 1 percent of the rotor blade height could be

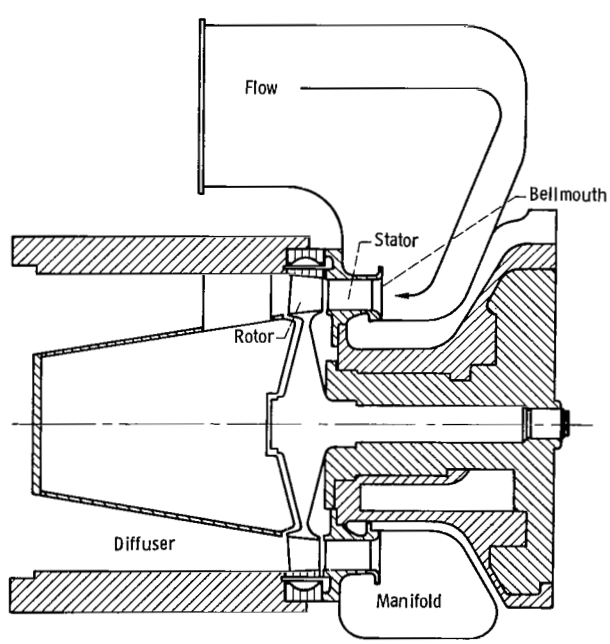


Figure 1. - Turbine cross-sectional schematic.

TABLE I.—TURBINE DESIGN PARAMETERS

| Parameter | Actual | Equivalent | Test conditions |
|---|---|---|---|
| Turbine inlet temperature, K | 501.7 | 288.2 | 322 |
| Turbine inlet pressure, $N/cm^2$ | 31.8 | 10.1 | 13.8 |
| Mass flow rate, kg/sec | 0.828 | 0.348 | 0.448 |
| Rotative speed, rpm | 43 893 | 33 267 | 35 178 |
| Specific work, J/g | 114.2 | 65.6 | 73.3 |
| Torque, N-m | 20.6 | 6.5 | 8.8 |
| Power, kW | 94.5 | 22.8 | 32.8 |
| Total to total pressure ratio, $P_1'/P_3'$ | 2.84 | 2.84 | 2.84 |
| Total to static pressure ratio, $P_1'/P_3$ | 3.10 | 3.10 | 3.10 |
| Total to static pressure ratio, $P_0'/P_4$ | 3.14 | 3.14 | 3.14 |
| Total efficiency, $\eta_{1-3}'$ | 0.880 | 0.880 | 0.880 |
| Static efficiency, $\eta_{1-3}$ | 0.819 | 0.819 | 0.819 |
| Static efficiency, $\eta_{0-4}$ | 0.812 | 0.812 | 0.812 |
| Work factor, $\Delta V_u/U_m$ | 1.47 | 1.47 | 1.47 |
| Reynolds number, $w/\mu r_m$ | $5.1\times10^5$ | $3.2\times10^5$ | $3.7\times10^5$ |
| Blade-jet speed ratio, $\nu_{1-3}$ | 0.524 | 0.524 | 0.524 |
| Blade-jet speed ratio, $\nu_{0-4}$ | 0.522 | 0.522 | 0.522 |

TABLE II.—TURBINE DESIGN PHYSICAL PARAMETERS

| Parameter | Stator | Untwisted, 37-blade rotor | Untwisted, 43-blade rotor | Twisted 43-blade rotor |
|---|---|---|---|---|
| Actual chord,[a] cm | 2.490 | 1.592 | 1.493 | 1.493 |
| Axial chord,[a] cm | 1.693 | 1.405 | 1.438 | 1.438 |
| Leading-edge radius, cm | 0.166 | 0.104 | 0.030 | 0.030 |
| Trailing-edge radius, cm | 0.021 | 0.015 | 0.013 | 0.013 |
| Radius, cm: | | | | |
| Hub | 5.32 | [b]5.18 | [b]5.18 | [b]5.18 |
| Mean | 6.02 | [b]6.02 | [b]6.02 | [b]6.02 |
| Tip | 6.72 | [b]6.87 | [b]6.87 | [b]6.87 |
| Blade height, cm | 1.40 | 1.56 | 1.56 | 1.56 |
| Solidity,[a] $\sigma$ | 1.51 | 1.56 | 1.70 | 1.70 |
| Aspect ratio, $AR$ | 0.56 | 0.98 | 1.06 | 1.06 |
| Number of blades | 23 | 37 | 43 | 43 |
| Radius ratio | 0.79 | 0.77 | 0.77 | 0.77 |
| Blade pitch,[a] cm | 1.64 | 1.02 | 0.88 | 0.88 |

[a]Values at mean section.
[b]Values at rotor exit.

used. The turbine exit section was designed to diffuse the flow.

The actual design conditions, the equivalent design conditions, and the test conditions for this turbine are shown in table I. The turbine was designed for an efficiency of 0.88 at a work factor of 1.47. Some of the physical parameters for this turbine are listed in table II. The stator had 23 blades; the stator blade height and aspect ratio were 1.40 centimeters and 0.56, respectively. As mentioned in the Introduction three rotor configurations were evaluated in this investigation. Besides the original untwisted, 37-blade rotor, an untwisted, 43-blade rotor and a twisted, 43-blade rotor were evaluated. Both 43-blade rotor designs had a solidity of 1.70, as compared with 1.56 for the 37-blade rotor design. The 43-blade rotor designs also had much thinner leading edges.

The mean-section velocity diagram is shown in figure 2. The stator discharge angle was 73°, but the rotor was designed for zero exit swirl. The mean rotor reaction $R_x$ was 0.21.

The manifold and stator assembly and the rotor configurations evaluated are shown in figures 3 and 4, respectively. Figure 5 shows the three types of honeycomb shrouds evaluated. Each rotor configuration had its own shroud. The original honeycomb shroud, denoted as the open honeycomb, had a cell diameter of 0.16 centimeter and a cell depth of 0.38 centimeter. The second honeycomb shroud, denoted as the half-depth honeycomb, had the same cell diameter but a cell depth of only 0.19 centimeter. Each of the open honeycomb shrouds was filled to produce a solid shroud surface configuration, which was denoted as the filled honeycomb. The purpose of testing these three shroud configurations was to quantify the variation of turbine efficiency with honeycomb depth.

## Research Equipment and Procedure

The apparatus used in this investigation consisted of the research turbine, an airbrake dynamometer

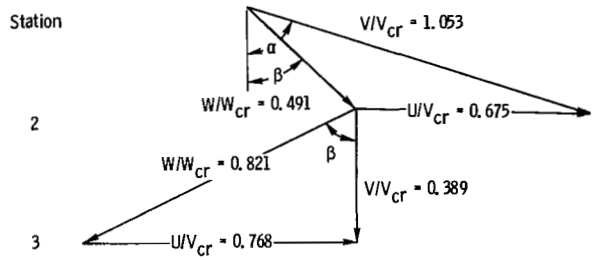


| Station | Absolute gas angle, α, deg | Relative gas angle, β, deg |
|---|---|---|
| 2 | 73 | 47.2 |
| 3 | 0 | -63.1 |

Figure 2. - Mean-section velocity diagram.

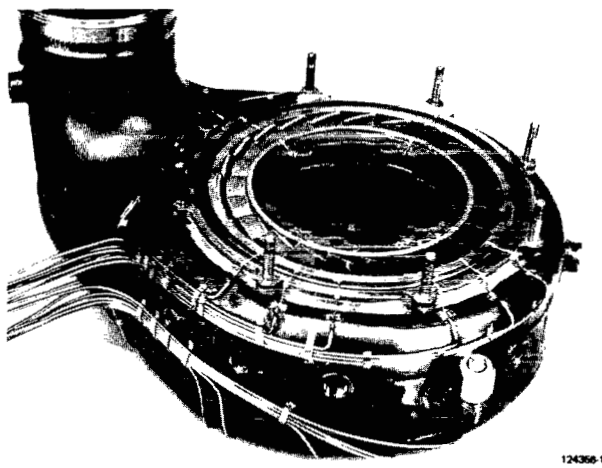


Figure 3. - Manifold and stator assembly.

used to control the speed and absorb and measure the power output of the turbine, an inlet and exhaust piping system including flow controls, and appropriate instrumentation. A schematic of the experimental equipment is shown in figure 6. The rotational speed of the turbine was measured with an electronic counter in conjunction with a magnetic pickup and a shaft-mounted gear. Mass flow was measured with a calibrated venturi. Turbine torque was determined by measuring the reaction torque of the airbrake, which was mounted on air trunnion bearings, and adding corrections for tare losses, which were the turbine bearings and seal losses and the coupling windage. These tare losses corresponded to about 4.0 percent of the measured torque obtained at design equivalent speed and design blade-jet speed ratio. The torque load was measured with a commercial strain-gage load cell.

The turbine instrumentation stations are shown in figure 7. Instrumentation at the manifold inlet (station 0) measured wall static pressure and total temperature. Static pressures were obtained from two taps located 180° apart. Total temperature was measured with three thermocouple probes that were located at approximately 10, 50, and 90 percent of the pipe diameter.

At the bellmouth inlet (station 1) total pressure and flow angle were measured at four circumferential locations with the survey probe shown in figure 8. At each circumferential location data were obtained at several radial positions ranging from about −7 to 115 percent of the stator blade height. At each position the survey probe remained fixed and the flow angle and total pressure were obtained from probe measurements and calibration curves.

At the stator exit (station 2), less than half an axial chord length downstream of the stator, static pressures were measured with 16 taps, eight each on

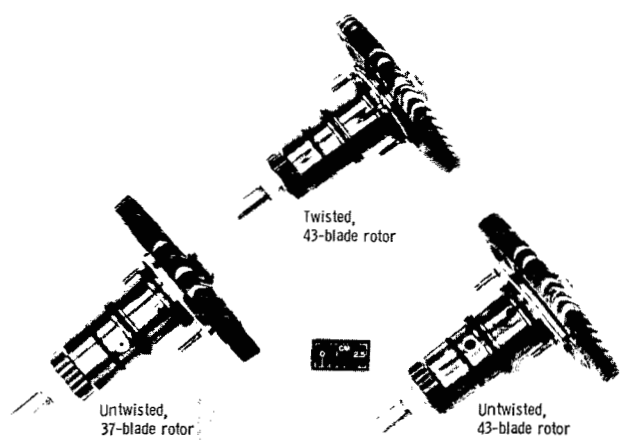


Figure 4. - Rotor configurations tested. C-80-1291

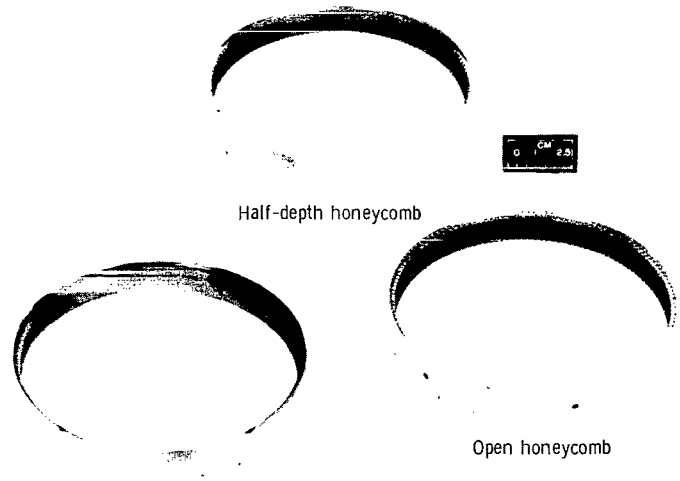


Figure 5. - Honeycomb shroud configurations.

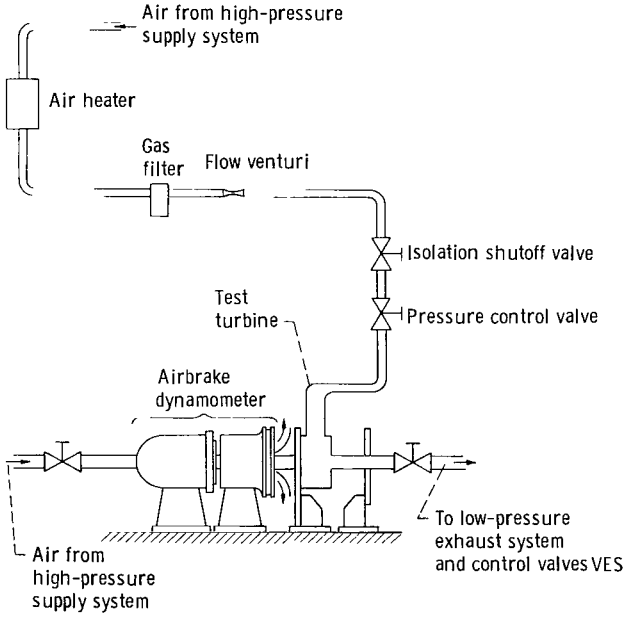


Figure 6. - Experimental equipment schematic.

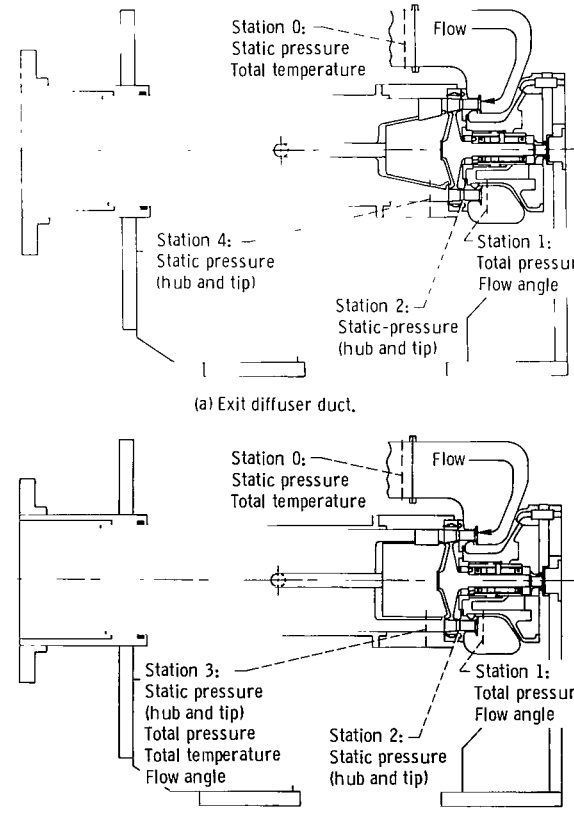


(a) Exit diffuser duct.

(b) Constant-area exhaust duct.

Figure 7. - Turbine instrumentation.

the inner and outer walls. The inner and outer wall taps were located opposite each other at different intervals around the circumference.

As shown in figure 7 two different exhaust ducts were used. To obtain turbine performance data including the diffuser, the exit diffuser duct shown in figure 7(a) was used. Blading performance was obtained by replacing the exit diffuser duct with a

constant-area exhaust duct (fig. 7(b)). Using a constant-area exhaust duct allowed the rotor exit instrumentation to be located at a position where the rotor wakes were mixed out without being affected by the diffusion process. This position was determined by using a hot-wire anemometer survey probe at several axial locations downstream of the rotor. For this turbine this position was approximately 1½ axial chord lengths downstream of the rotor.

C-80-1293

Figure 8. - Bellmouth inlet survey probe.

At the rotor exit (station 3) static pressure, total pressure, total temperature, and flow angle were measured. The static pressure was measured with eight taps, four each on the inner and outer walls. These inner and outer wall taps were located opposite each other at 90° intervals around the circumference. Three self-aligning probes located at three positions around the circumference were used to measure total pressure, total temperature, and flow angle. The rotor exit survey probe and actuator are shown in figure 9.

At the diffuser exit (station 4) static pressure was measured with eight taps, four each on the inner and outer walls. These inner and outer wall taps were located opposite each other at 90° intervals around the circumference.

The experimental program consisted of an evaluation of both the stator and the stage. The stator evaluation included both bellmouth inlet and stator exit surveys. The bellmouth inlet surveys were discussed earlier. For the stator exit surveys the rotor was removed and the survey probe shown in figure 10 was used to obtain total pressure and flow angle over a range of circumferential and radial positions. Figure 11 shows the bellmouth inlet and stator exit survey circumferential locations. Each of the four stator exit survey sectors consisted of two consecutive stator blade spacings (31.3°). In each sector data were obtained approximately every 1.2° at radial positions equal to approximately 10, 30, 50, 70, and 90 percent of the stator blade height. For each data point the probe remained fixed and the total pressure

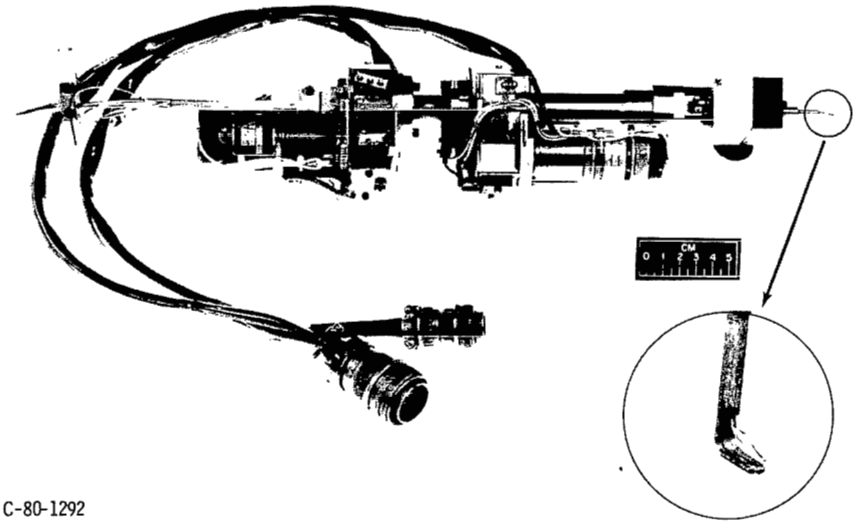


C-80-1292

Figure 9. - Rotor exit survey probe and actuator.

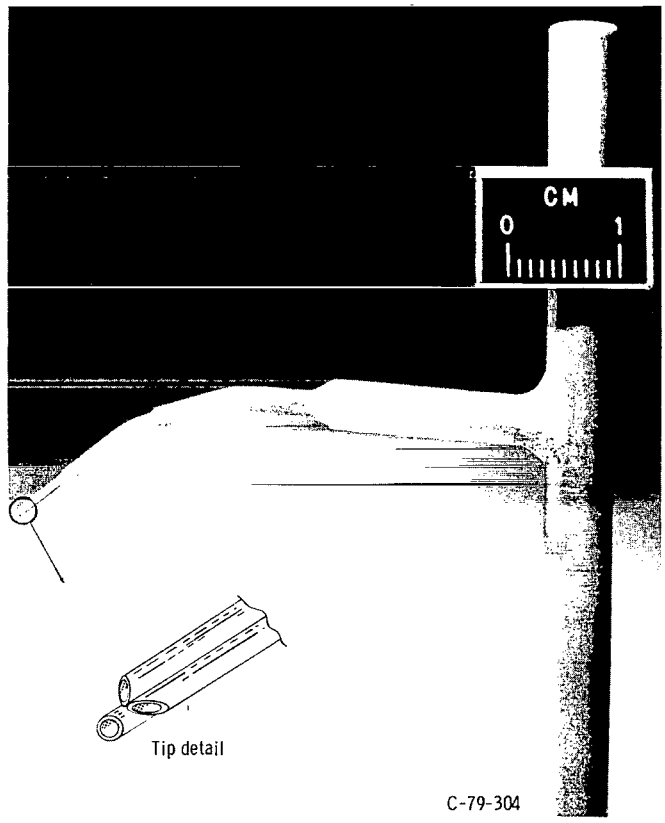


Figure 10. - Stator exit survey probe.

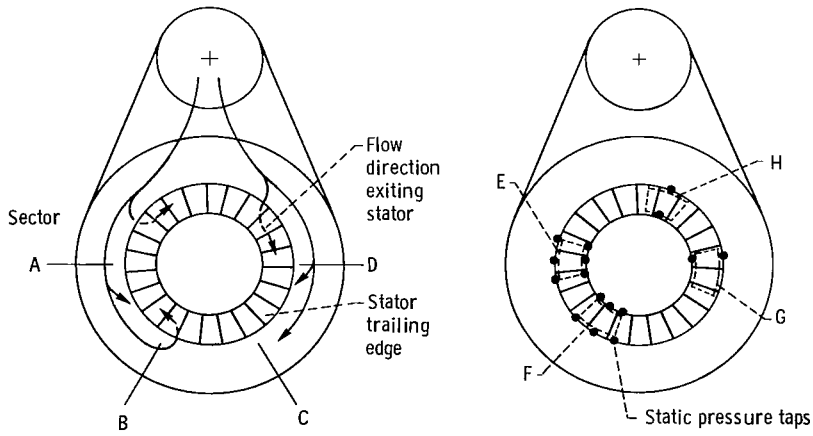


(a) Bellmouth inlet survey locations. (b) Stator exit survey sectors.

Figure 11. - Bellmouth inlet and stator exit survey locations (view looking into manifold).

and flow angle were obtained from probe readings and calibration curves. The survey data obtained at a given radial position were then arithmetically averaged. Both the bellmouth inlet and stator exit surveys were conducted at the design manifold-inlet- to stator-exit-mean-static-pressure ratio of 2.2.

For the stage evaluation data were obtained at nominal inlet total flow conditions of 322 K and 13.8 $N/cm^2$. The turbine Reynolds number at these conditions was about $3.7 \times 10^5$, which was considered high enough to avoid any effect of Reynolds number on performance. Initially, the exit diffuser duct was installed and performance data were obtained over a range of manifold-inlet-total- to diffuser-exit-static-pressure ratio from 1.60 to 4.60 and over a range of design equivalent speeds from 30 to 110 percent. All three rotors were tested with the exit diffuser duct installed. The constant-area exhaust duct was then installed. Data were obtained for the three rotor configurations over a range of bellmouth-inlet-total- to rotor-exit-static-pressure ratios from 1.55 to 4.50 and over a range of design equivalent speeds from 30 to 110 percent.

The turbine was rated on the basis of both total and static efficiency. The actual work was calculated from torque, speed, and mass flow measurements. The manifold inlet total and rotor exit total pressures used in determining the efficiencies were calculated from mass flow, static pressure, total temperature, and flow angle. At the manifold inlet the flow angle was assumed to be zero. The bellmouth inlet total pressure was based on an arithmetic average of the bellmouth inlet survey results.

## Results and Discussion

### Stator Survey Results

The bellmouth inlet survey results are shown in figure 12. As mentioned in the section Research Equipment and Procedure the bellmouth inlet surveys were conducted at radial positions from about −7 to 115 percent of the stator blade height at four circumferential positions (fig. 11).

Figure 12 shows that the bellmouth-inlet- to manifold-inlet-total-pressure ratio was about 0.98 around the circumference. Because the flow entering the manifold impacted the elbow section before being turned 180° into the stator (fig. 1), about 50 percent of the velocity head was lost. In addition, the total pressure ratio decreased from the hub to the tip at each circumferential position. This trend was

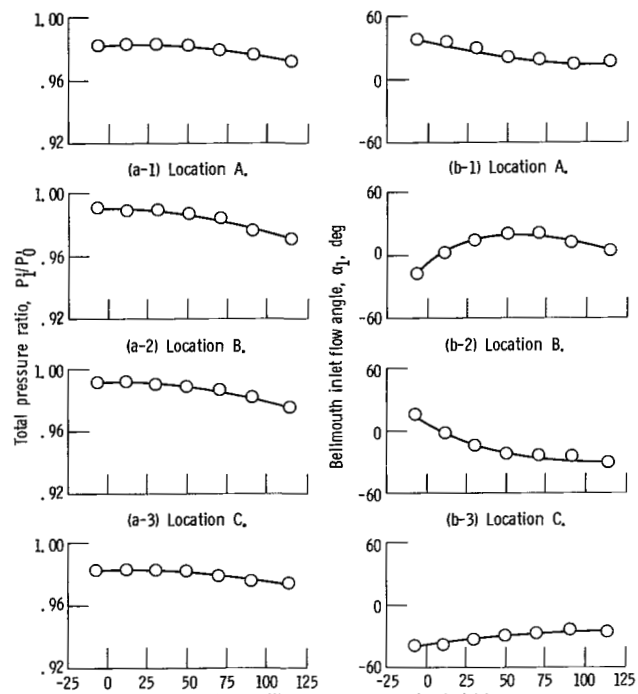


(a) Total pressure ratio. (b) Bellmouth inlet flow angle.

Figure 12. - Bellmouth inlet survey results.

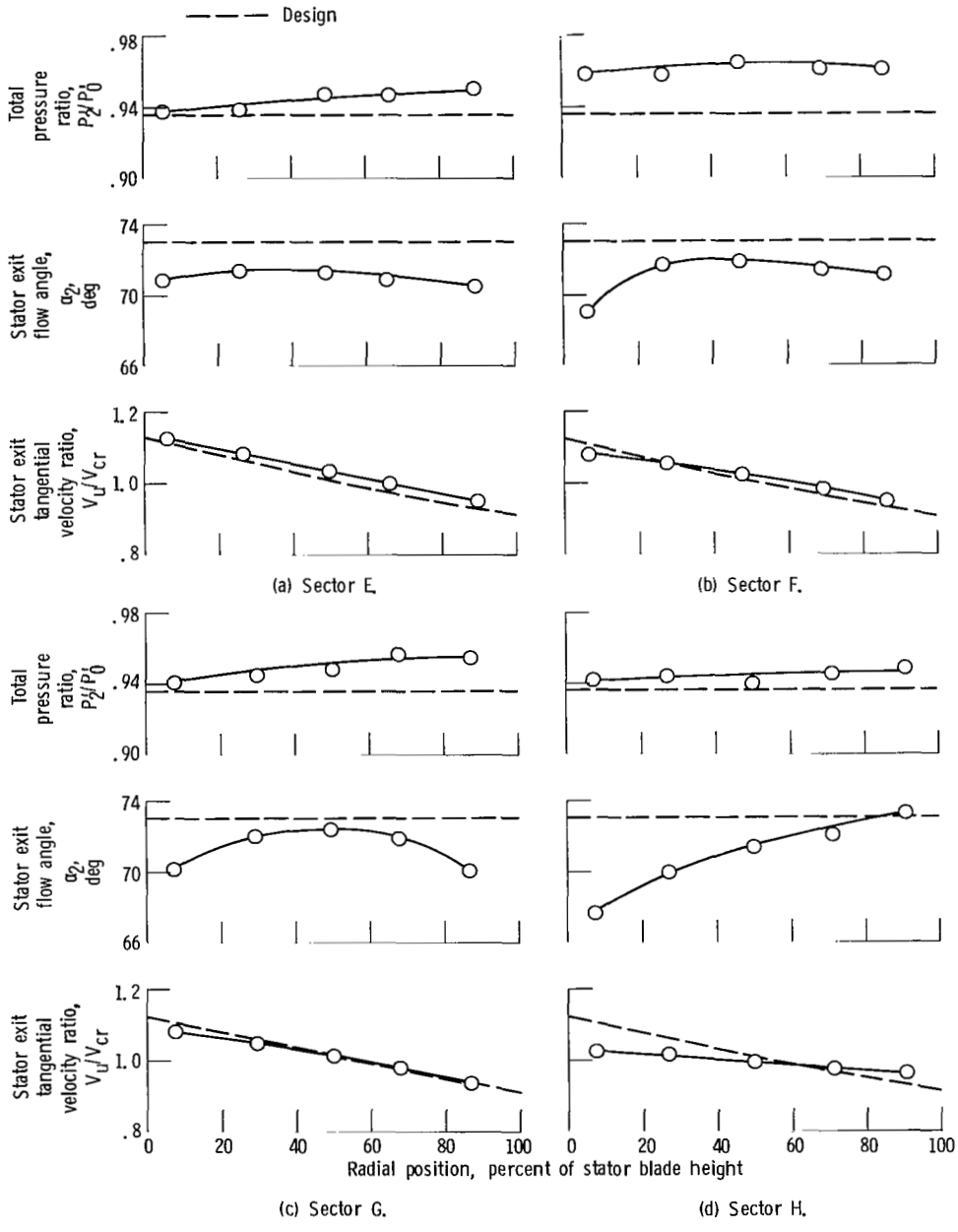


Figure 13. - Stator exit survey results.

attributed to a probe pitch angle effect as the probe was moved radially toward the tip into a region where high radial components of flow existed. Since the survey probe was not calibrated for a pitch angle greater than 10°, the total pressure obtained from the calibration curve would have been less than the true total pressure. However, even if it were assumed that the total pressure ratio had remained constant near the tip instead of decreasing, this would have had only a small effect on the average value. Thus the probe pitch effect was not considered to be detrimental.

Also indicated by figure 12 is a circumferential variation in the level of total pressure. The total pressure ratio was about 0.5 percent higher near the bottom of the manifold (locations B and C) than at the sides (locations A and D). Although this trend was unexpected, the amount of variation was considered small and no further investigation of this trend was made.

An arithmetically averaged total pressure ratio was calculated at each of the four locations surveyed, and then those four averages were combined into a single overall average. The overall average was 0.983, which was also the design value. This value of 0.983 was subsequently used in the stage tests to determine the bellmouth inlet total pressure from the manifold inlet total pressure.

Figure 12 also shows a wide radial and circumferential variation in the bellmouth inlet flow angle. Since the design bellmouth inlet flow angle was 0°, it is evident that the stator experienced incidence angles ranging from −40° to 40°. The effect of this incidence angle variation was expected to be small since the critical velocity ratio at the stator inlet was only about 0.2.

The stator exit survey results are shown in figure 13. Test data obtained by the manufacturer indicated a high loss area near sector E (fig. 11). The stator exit surveys were made to determine whether this or any other major loss area existed.

As with the bellmouth inlet survey results the stator exit surveys indicated radial and circumferential variations in total pressure and flow angle. The highest total pressure was near the bottom of the manifold (sector F), which was consistent with the bellmouth inlet results. Arithmetically averaging the total pressure ratio and flow angle data resulted in values of 0.950 and 71°. The corresponding design values were 0.936 and 73°. The survey results at each circumferential position were used to calculate stator exit tangential velocity ratios, which are also shown in figure 13. The results indicated that the radial variations in tangential velocity ratio at the four survey sectors were close to the design intent. From the results shown in figure 13 it was determined that even though there were radial and circumferential gradients in flow, no large loss areas existed in the stator.

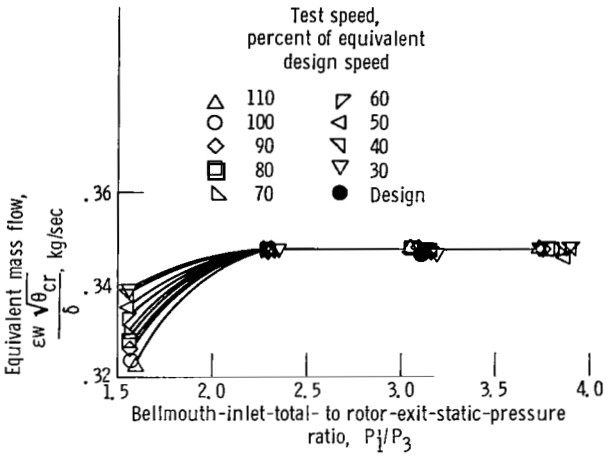


Figure 14. - Variation of mass flow with pressure ratio.

## Stage Results

Equivalent mass flow is plotted against turbine pressure ratio in figure 14. Beyond a pressure ratio of about 2.3 a stator choke condition existed. The choking mass flow was 0.349 kg/sec, which was 0.3 percent higher than design. Since a stator choke condition existed, the mass flow was unaffected by the rotor configuration. Therefore the mass flow trend shown in figure 14 was typical for all the rotor and shroud configurations evaluated. A summary of the turbine efficiencies obtained at design equivalent conditions of speed and blade-jet speed ratio is presented in table III for all the rotor and shroud configurations evaluated in the stage investigation.

Initially the three rotor configurations were evaluated with the exit diffuser duct and the original

TABLE III.—STAGE RESULTS SUMMARY

[Results at design equivalent conditions of design speed and blade-jet speed ratio.]

| Rotor configuration | Static efficiency, (honeycomb open) $\eta_{0-4}$ | Total efficiency, $\eta'_{1-3}$ | | |
|---|---|---|---|---|
| | | Honeycomb open | Honeycomb filled | Half-depth honeycomb |
| Untwisted, 37-blade rotor | 0.758 | 0.786 | 0.868 | 0.850 |
| Untwisted, 43-blade rotor | .750 | .785 | .871 | ---- |
| Twisted, 43-blade rotor | .725 | .773 | .883 | ---- |

honeycomb shroud installed. The performance results are shown in figure 15. Static efficiency, based on the manifold-inlet-total- to diffuser-exit-static-pressure ratio, is plotted against blade-jet speed ratio. At design equivalent conditions of speed and blade-jet speed ratio the static efficiencies were 0.758, 0.750, and 0.725 for the untwisted, 37-blade, the untwisted, 43-blade, and the twisted, 43-blade rotor configurations, respectively. These efficiencies ranged from 5.4 to 8.7 points lower than the design value of 0.812.

The performance results for the three rotor configurations with the constant-area exhaust duct and the original honeycomb shroud installed are shown in figure 16. Total efficiency, based on the bellmouth-inlet- to rotor-exit-total-pressure ratio, is plotted against blade-jet speed ratio. At design equivalent conditions of speed and blade-jet speed ratio, the total efficiencies were 0.786, 0.785, and 0.773 for the untwisted, 37-blade, the untwisted, 43-blade, and the twisted, 43-blade rotor configurations, respectively. These efficiencies ranged from 9.4 to 10.7 points lower than the design value of 0.88.

Both the manufacturer and the Lewis Research Center believed that the turbine efficiency would be higher with the untwisted, 43-blade rotor than with the untwisted, 37-blade rotor because of higher rotor solidity. Similarly, the highest efficiency was expected with the twisted, 43-blade rotor because of higher rotor solidity and more optimum rotor incidence. Figures 15 and 16 reveal that neither of these expectations was fulfilled. It is likely that the improvements that were expected were masked by the large loss mechanism that caused the turbine efficiencies to be considerably less than design.

The dramatic improvement in turbine efficiency that occurred when the honeycomb shroud was filled is shown in figure 17. As before, turbine efficiency is plotted against blade-jet speed ratio. At design equivalent conditions of speed and blade-jet speed ratio the total efficiencies were 0.868, 0.871, and 0.883 for the untwisted, 37-blade, the untwisted, 43-blade, and the twisted, 43-blade rotor configurations, respectively. These efficiencies ranged from 8.2 to 11.0 points higher than with the honeycomb shroud unfilled. It is apparent that the open honeycomb shroud caused a massive loss mechanism to occur.

Comparing figures 16 and 17 shows that the largest efficiency improvement (11.0 points) occurred with the twisted, 43-blade rotor. This implied that the open honeycomb shroud degraded the stage performance more for this rotor configuration than for the other two rotor configurations. As shown in figure 18 a higher level of rotor reaction was obtained for the twisted rotor design than for the two

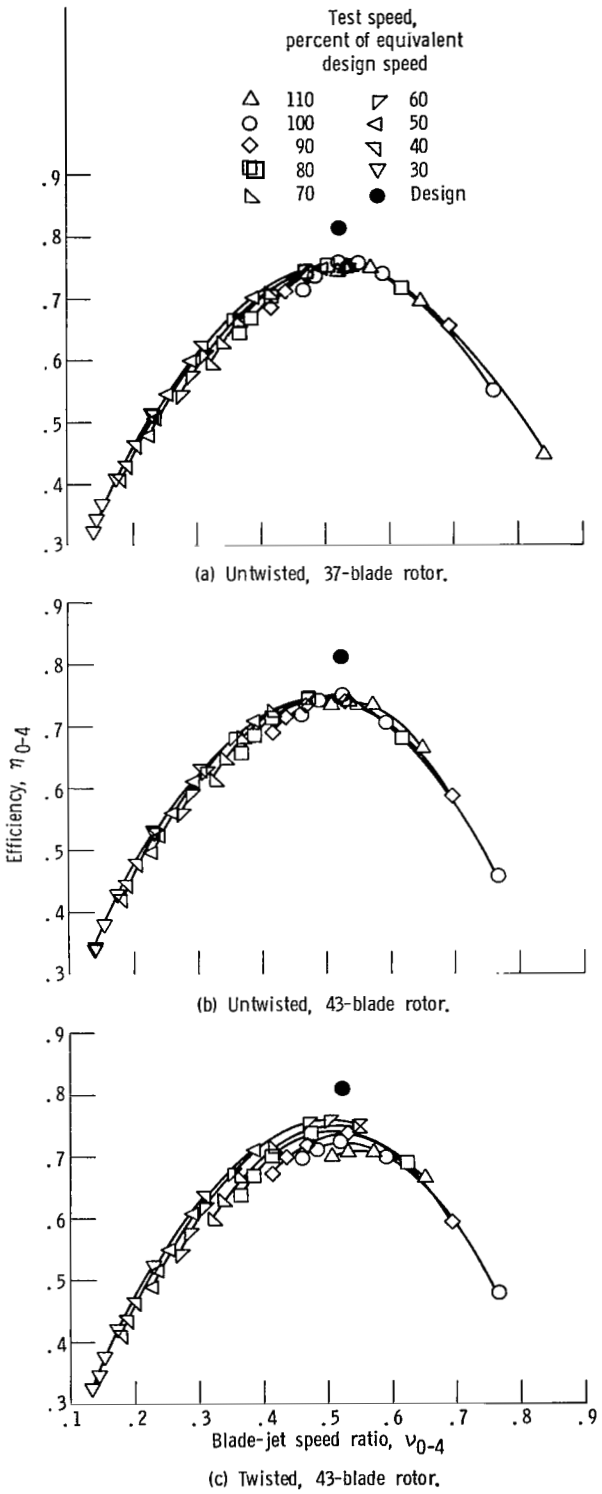


(a) Untwisted, 37-blade rotor.

(b) Untwisted, 43-blade rotor.

(c) Twisted, 43-blade rotor.

Figure 15. - Variation of efficiency with blade-jet speed ratio with exit diffuser duct installed and with open honeycomb shroud.

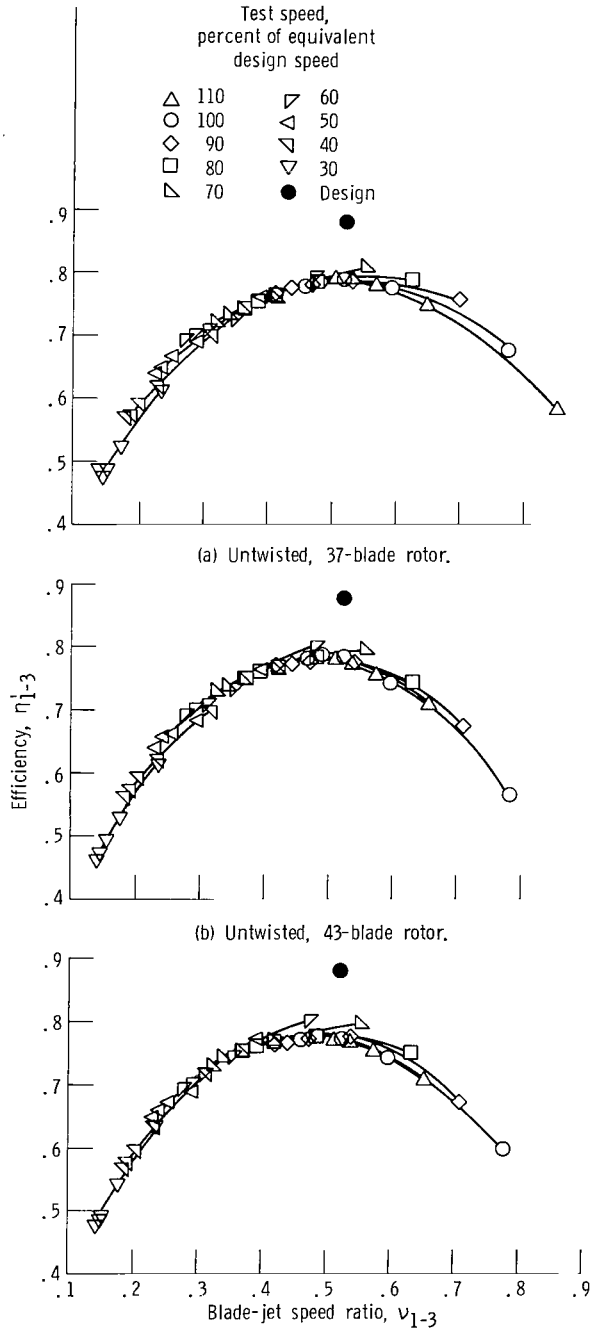


(a) Untwisted, 37-blade rotor.

(b) Untwisted, 43-blade rotor.

(c) Twisted, 43-blade rotor.

Figure 16. - Variation of efficiency with blade-jet speed ratio with constant-area exhaust duct installed and with open honeycomb shroud.

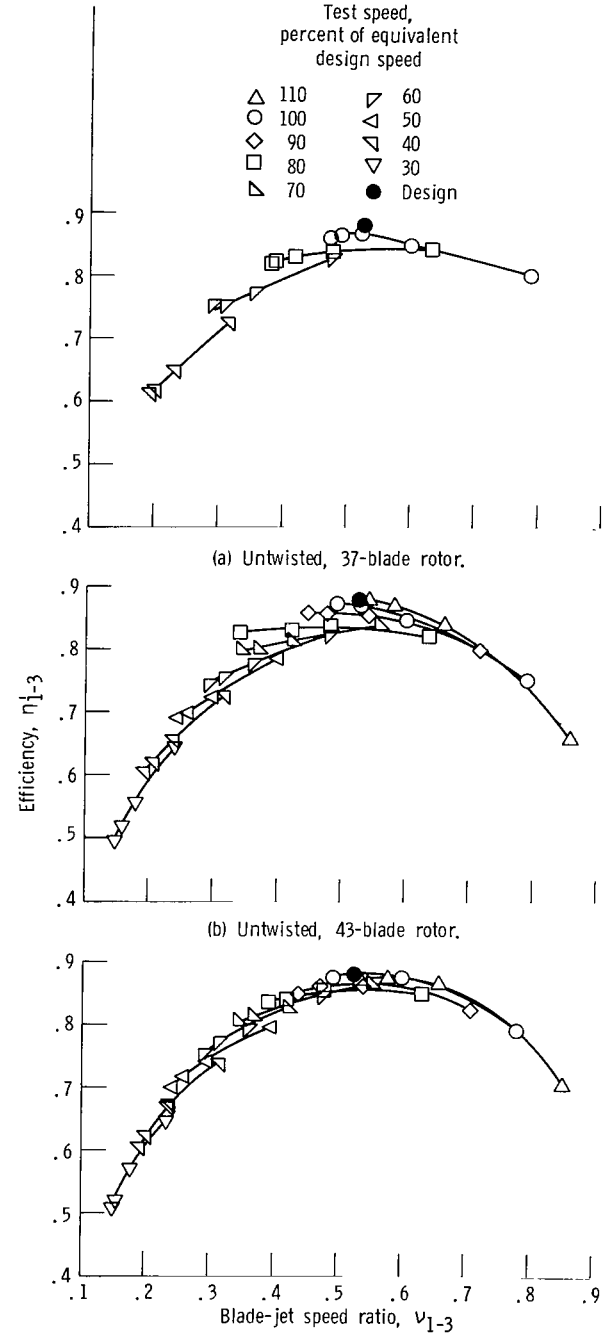


(a) Untwisted, 37-blade rotor.

(b) Untwisted, 43-blade rotor.

(c) Twisted, 43-blade rotor.

Figure 17. - Variation of efficiency with blade-jet speed ratio with constant-area exhaust duct installed and honeycomb shroud filled.

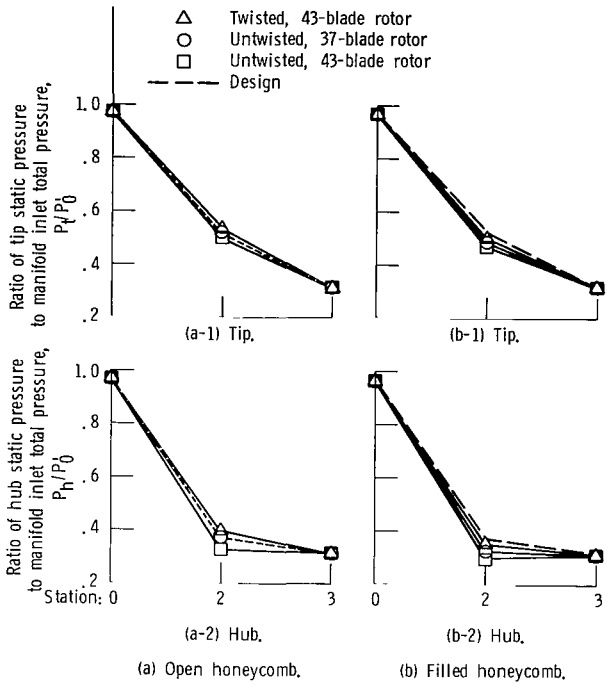


Figure 18. - Variation of static pressure through turbine at design equivalent speed.

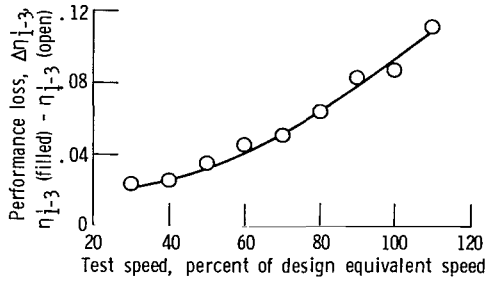


Figure 19. - Performance loss between filled and open honeycomb shroud configurations for untwisted, 43-blade rotor at design blade-jet speed ratio.

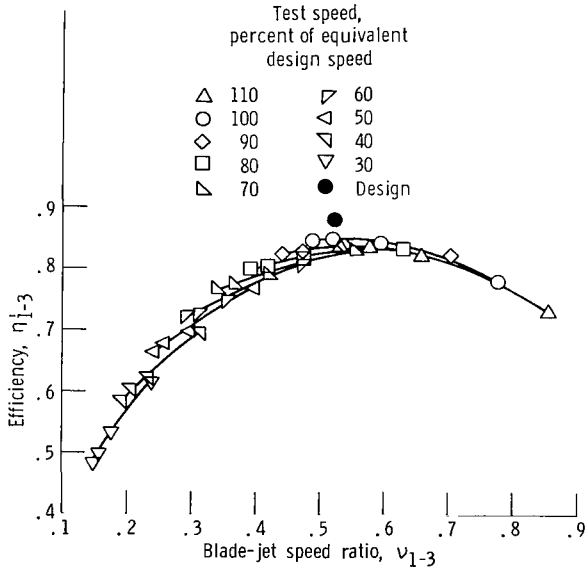


Figure 20. - Variation of efficiency with blade-jet speed ratio with half-depth honeycomb shroud installed - untwisted, 37-blade rotor configuration.

untwisted rotor designs for both the open and filled honeycomb shroud configurations. This difference in rotor reaction would suggest that, as compared with the two untwisted rotor configurations, the rotor inlet absolute tangential velocity was lower and the rotor exit absolute tangential velocity was higher for the twisted rotor configuration. Therefore, since the rotor exit absolute tangential velocity was a bigger contributor to the work output for the twisted rotor configuration, the performance loss caused by the open honeycomb shroud was more severe. In addition, figures 16 and 17 show that the performance loss for the open honeycomb shroud was not constant for each speed line tested. In fact, as shown in figure 19 for the untwisted, 43-blade rotor configuration, the performance loss between the unfilled and filled shroud configurations decreased with decreasing speed for operation at constant blade-jet speed ratio.

To obtain additional data on the performance degradation due to the honeycomb, a second honeycomb shroud was fabricated. This second shroud had the same cell diameter as the original, but the cell depth was halved. This new shroud was evaluated with the untwisted, 37-blade rotor installed. The performance results are presented in figure 20. At design equivalent values of blade-jet speed ratio and speed the turbine total efficiency was 0.850. This efficiency was 6.4 points higher than with the original honeycomb shroud installed and 1.8 points lower than with the filled honeycomb shroud installed. As compared with the original honeycomb shroud the percentage increase in efficiency with the half-depth honeycomb shroud installed was greater than the percentage change in the honeycomb cell depth.

Rotor exit radial surveys of total temperature, total pressure, and flow angle were conducted at design equivalent values of speed and blade-jet speed ratio to determine variations in blade element performance. Three survey probes were located downstream of the rotor at three different circumferential positions. The results from the probes were then arithmetically averaged. Figure 21 shows the averaged rotor exit survey results for the

untwisted, 37-blade rotor operating with each of the three shroud configurations. There are significant differences in the radial variations of the flow parameters among the three shroud configurations. The absolute levels of turbine efficiency calculated from the survey data (fig. 21(d)) are not as accurate as those based on the measured turbine torque, primarily because conduction made it difficult to obtain accurate total temperature measurements. However, the radial variations and relative levels of turbine efficiency calculated from the survey data are considered adequate to reveal significant differences in the blade element performance. These results show that the honeycomb shrouds affected not just the flow locally near the tip, but also the flow across the entire blade span. Figures 21(b) and (c) show that the radial variations in total temperature and total pressure were more nearly constant for the filled honeycomb shroud than for the two open honeycomb shrouds. The most dramatic efficiency improvement occurred with the filled honeycomb shroud as shown in figure 21(d). The efficiency for the filled honeycomb was higher across the entire blade span than that for the open honeycomb. The biggest difference was near the midspan, where a large loss area existed for the open honeycomb. For the half-depth honeycomb this midspan loss area was still present, although not as severe.

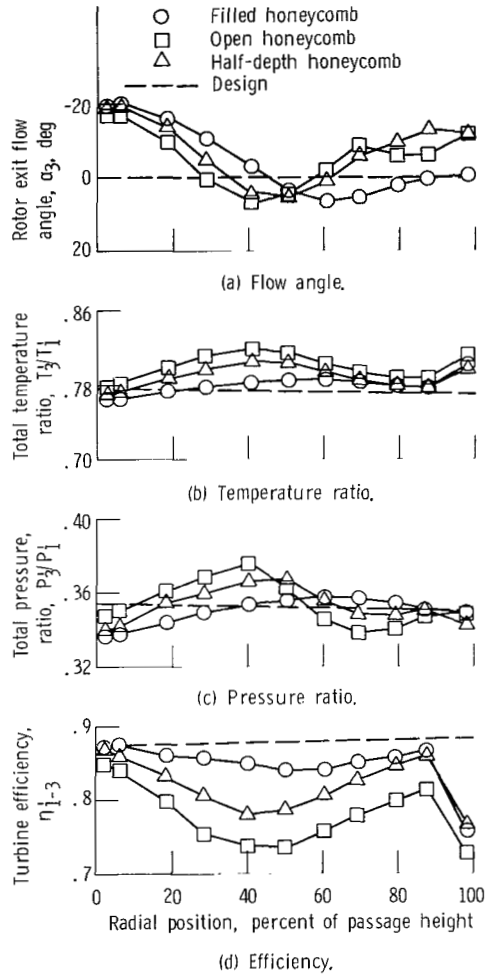


Figure 21. - Rotor exit survey results - untwisted, 37-blade rotor configuration.

## Kulite Probe Results

The rotor exit survey results showed that a large loss extending over most of the rotor blade occurred with the rotor operating with an open honeycomb shroud. To obtain an understanding of this loss mechanism, a high-frequency-response Kulite probe was installed in both the open and filled honeycomb shrouds near the mid-axial chord location. The Kulite probe measured the rotor tip static pressure variation across the rotating blade passages at this mid-axial chord location. These pressure measurements were taken over a range of turbine speed and were analyzed to obtain insight into the honeycomb shroud performance loss.

The Kulite probe results for the untwisted, 43-blade rotor are shown in figure 22. The data presented in figure 22(a) were obtained with the Kulite probe installed in one cell of the filled honeycomb shroud and flush with the shroud surface. The peak-to-peak pressure values are an indication of the pressure differential between the suction and pressure sides of the blade at the tip midchord location. The data shown in figure 22(b) were obtained with the Kulite probe placed at the bottom of one cell in the open honeycomb shroud so that the transducer sensed the pressure variations at the bottom of the cavity. For both figures 22(a) and (b) data were obtained at 40, 60, 80, and 100 percent of equivalent design speed.

Figure 22 shows that the magnitude of the peak-to-peak pressures varied from about 40 to 60 percent of the average pressure. In addition, although the peak-to-peak pressure values changed for both cases as speed changed, these pressure changes were small.

The following flow model was hypothesized on the basis of the results shown in figure 22: As the rotor blade passed by each cell in the honeycomb shroud, there was a rise in the static pressure. As a result a finite amount of gas flowed into the cell. After the maximum static pressure was reached, the pressure began to decrease, a sign that flow had exited the cell. The absolute velocity of this flow was normal to the mainstream flow direction. This flow out of the cell continued until the adjacent blade approached. This cyclic exchange of mass flow was repeated 43 times for each revolution of the rotor. The amount of gas

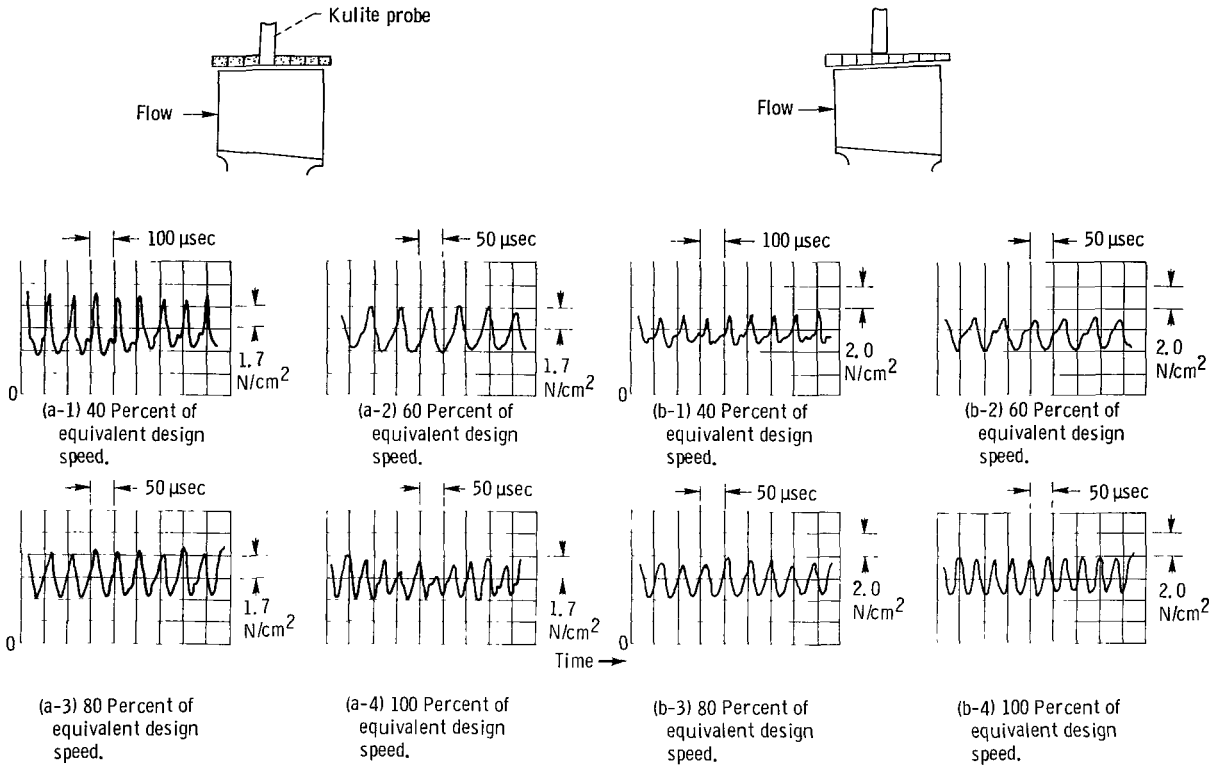


Figure 22. - Results of tests with pressure probe installed in honeycomb shroud of untwisted, 43-blade rotor.

flowing into and out of the cells was theorized to be proportional to the cell volume and the average peak-to-peak pressure within the cell. The mass flow rate was then proportional to the amount of gas flowing into and out of the cells per passing blade and the blade passing frequency. Thus there was a trend of increasing mass flow rate with increasing rotative speed.

The gas being transported into and out of the honeycomb cells caused an efficiency loss. The transported gas lost kinetic energy in entering and leaving the cell. This flow reentered the primary mainstream with zero absolute tangential and axial velocity. Thus energy from the rotor and the primary mainstream was required to energize this fluid. In addition, the mainstream flow velocity was reduced in mixing with the transported gas, and thus a region of low-momentum fluid was formed, the effect of which was propagated radially and caused a large loss to occur over most of the blade height. The amount and extent of this loss would of course vary with the amount of transported gas. Thus, reducing the honeycomb cell depth or reducing the turbine rotative speed would reduce the performance deficit for an open honeycomb shroud.

# Concluding Remarks

The results obtained in this experimental investigation showed that the use of an open honeycomb shroud caused the large performance deficit for the aircraft engine starter turbine. Although the loss mechanism associated with the honeycomb shroud is not fully understood, there is no doubt that the use of this shroud in this turbine application is not desirable. It is possible that a honeycomb shroud configuration exists in which the performance loss would be minimized. However, the results of this program could not be used to determine what this optimum configuration would be.

The efficiencies that were achieved when the honeycomb shrouds were filled were considered excellent for a turbine of this size and work factor. Although no stator inlet boundary layer measurements were made, it was believed that the use of the short bellmouth inlet with its resultant thin boundary layers was an important contributor to these efficiency levels.

## Summary of Results

An experimental investigation was conducted on a 13.5-centimeter-tip-diameter aircraft engine starter turbine to determine the reasons for its low aerodynamic performance. The investigation consisted of an evaluation of both the stator and the stage. The investigation focused on determining the effect on the aerodynamic performance of two turbine design features: the use of a manifold having a single inlet and designed to turn the flow 180° into the stator, and the use of a honeycomb shroud surface over the rotor blade tips. Three rotor configurations and three honeycomb shroud configurations were evaluated. The three rotor configurations consisted of an untwisted, 37-blade rotor, an untwisted 43-blade rotor, and a twisted, 43-blade rotor. The three honeycomb shroud configurations consisted of the original shroud, a filled shroud, and a half-depth shroud. The results of this investigation can be summarized as follows:

1. When the original honeycomb shroud configuration was filled to obtain a solid shroud surface, efficiency improvements ranging from 8.2 to 11.0 points were obtained for the three rotor configurations. As a result the total efficiencies ranged from 0.868 to 0.883.

2. The large loss associated with use of an open honeycomb shroud was believed to be due primarily to the energy loss associated with gas being transported into and out of the honeycomb cells as a result of the blade-to-blade pressure differential at the tip section.

3. Although the manifold used in this turbine design caused large radial and circumferential gradients in flow, the stator exit surveys indicated that no large loss areas existed in the stator.

Lewis Research Center
National Aeronautics and Space Administration
Cleveland, Ohio, October 3, 1980

| | | |
|---|---|---|
| 1. Report No. NASA TP-1810<br>AVRADCOM TR-80-C-17 | 2. Government Accession No. | 3. Recipient's Catalog No. |
| 4. Title and Subtitle REASONS FOR LOW AERODYNAMIC PERFORMANCE OF 13.5-CENTIMETER-TIP-DIAMETER AIRCRAFT ENGINE STARTER TURBINE | | 5. Report Date<br>March 1981<br>6. Performing Organization Code<br>505-32-2B |
| 7. Author(s)<br>Jeffrey E. Haas, Richard J. Roelke, and Paul Hermann | | 8. Performing Organization Report No.<br>E-540<br>10. Work Unit No. |
| 9. Performing Organization Name and Address<br>NASA Lewis Research Center<br>and<br>Propulsion Laboratory<br>AVRADCOM Research and Technology Laboratories<br>Cleveland, OH 44135 | | 11. Contract or Grant No.<br>13. Type of Report and Period Covered<br>Technical Paper |
| 12. Sponsoring Agency Name and Address<br>National Aeronautics and Space Administration<br>Washington, DC 20546<br>and<br>U.S. Army Aviation Research and Development Command<br>St. Louis, MO 63166 | | 14. Sponsoring Agency Code |

15. Supplementary Notes Jeffrey E. Haas, AVRADCOM Research and Technology Laboratories; Richard J. Roelke, Lewis Research Center; Paul Hermann, Sundstrand Corp., Rockford, Ill. Presented in part at SAE Aerospace Meeting, Los Angeles, Calif., Oct. 13-16, 1980.

16. Abstract

An experimental investigation was made at the NASA Lewis Research Center to determine the reasons for the low aerodynamic performance of a 13.5-centimeter-tip-diameter aircraft engine starter turbine. The investigation consisted of an evaluation of both the stator and the stage. An approximate 10-percent improvement in turbine efficiency was obtained when the honeycomb shroud over the rotor blade tips was filled to obtain a solid shroud surface.

| | | | |
|---|---|---|---|
| 17. Key Words (Suggested by Author(s))<br>Honeycomb shroud; Starter turbine | 18. Distribution Statement<br>Unclassified - unlimited<br>STAR Category 07 | | |
| 19. Security Classif. (of this report)<br>Unclassified | 20. Security Classif. (of this page)<br>Unclassified | 21. No. of Pages<br>18 | 22. Price*<br>A02 |

* For sale by the National Technical Information Service, Springfield, Virginia 22161

NASA-Langley, 1981

National Aeronautics and Space Administration

Washington, D.C.
20546

SPECIAL FOURTH CLASS MAIL
BOOK

Postage and Fees Paid
National Aeronautics and
Space Administration
NASA-451


Official Bu
Penalty fo

11 1 1U,A, 030281 S00903DS
DEPT OF THE AIR FORCE
AF WEAPONS LABORATORY
ATTN: TECHNICAL LIBRARY (SUL)
KIRTLAND AFB NM 87117

NASA

POSTMASTER: If Undeliverable (Section 158 Postal Manual) Do Not Return